RSC Advances

ROYAL SOCIETY OF CHEMISTRY

www.rsc.org/advances

Journal Name

ARTICLE

Shear-induced self-assembly of linear ABC triblock copolymers in solutions: Creation of 1D cylindrical Micellar Structures†

Received 00th January 20xx,
Accepted 00th January 20xx

DOI: 10.1039/x0xx00000x

www.rsc.org/

Yang Zhou,*[a,§] Chun Zhou,[a,§] Xi He,[a,c] Xianggui Xue,[a] Wen Qian,[a] Shikai Luo,[a] and Honggang Xia*[b]

Though the creation of nanostructures from solution self-assembly of block copolymers is one of the most promising approaches, the formation of 1D cylindrical structures remains a challenge. In this work, the shear flow is introduced to create the 1D cylindrical micellar structures based on the solution self-assembly of linear ABC terpolymers. Dissipative particle dynamics method is used to explore the whole morphological space. Firstly, 7 spherical (0D), 10 cylindrical and 1 oblate spherical (1D), 5 lamella and 3 oblate cylindrical (2D) micellar strcutres are summarized from the total of 315 morphologies. Secondly, several 1D cylindrical micelles provided by this simulation have the potential to become the interesting single-, double-walled nanotube and the cylindrical co-micelles. Finally, the shear rate, the concentration and the solvophilic block length as three key factors of controlling the creation of multidimensional structures are given, which are propitious to the formation of 1D, 2D and 0D structures, respectively. In fact, this work uses a simple shear means to promote the reorientation and rearrange of self-assemble morphologies, and selectively builds 0D (dot), 1D (tube) or 2D (sheet) nanostructures. These results are helpful to understand the formation of complex micelles by the shear-induced self-assembly of linear ABC triblock copolymers and tailor the new 1D cylindrical morphologies through experiments.

1. Introduction

Self-assembly of block copolymers, in order to prepare well-defined nanostructures, has gained significant scientific interest during the last decades.[1] These exquisitely ordered nanostructures have potential applications in drug release,[2] microelectronic materials,[3] and so on. Recently, ABC triblock copolymers, which has two representative topological structures of linear (*l*-ABC) and star ABC (μ-ABC), have been rapidly paid more attention,[4] because of their expansive spectrum of accessible morphologies. Originally, concentric morphologies are generally regarded as the default structure adopted by *l*-ABC,[5] however, effectively suppressed by μ-ABC.[6] It leads to a vast array of fascinating morphologies.[4,7] Thus, most works had been focused on the self-assembly of μ-ABC, including several crucial simulation and theoretical studies.[8-13] Laschewsky and co-workers later revealed an inspiring result that *l*-ABC also form nonconcentric micelles.[14-18] In addition, Muller et al also found several novel micelles (vesicle, toroid, undulated ribbon) from *l*-ABC.[19] Obviously, the potential of the simple *l*-ABC is underestimated at one time. Subsequently, we utilized dissipative particle dynamics (DPD) simulations to explore the phase diagram of *l*-ABC in solution. Rich micelles (such as raspberry-onion, helix-on-sphere, etc.) beyond the traditional understanding are supplemented.[20-22] Furthermore, combining with other simulations and theories,[9,10,23-27] the knowledge on the self-assemble behaviours of linear ABC triblock copolymers have been evidently enriched.

Among all exquisitely morphologies, 1D nanostructures have attracted considerable attention, because of their wide potential application, such as the flow-intensive drug or dye delivery,[28] the liner scaffold for mineralization,[29,30] the template for creating linear arrays of nanoparticles,[31] and so on. Moreover, the preparation of 1D nanostructures by the self-assembly of block copolymers also become the hot-spot of this field. For example, Wang and co-workers utilized the diblock copolymer of polyferrocenyldimethylsilane (PFS) to build cylindrical micelles in solution and form co-micelles by adding a different block copolymer.[32] Through a combination of crystallization-driven self-assembly of block copolymers based on PFS and selective micelle corona cross-linking, Rupar et al created monodisperse cylindrical seed micelles (about 130nm) that grow unidirectionally.[33] He's group successfully prepared the nanotubular (hollow cylindrical) micelles via self-assembly of a poly (styrene-*b*-4-vinyl pyridine-*b*-ethylene oxide) triblock terpolymer in binary organic solvents with assistance of solution thermal annealing.[34] In fact, most diblock copolymers prefer to form spherical micelles than cylindrical micelles.[32] The investigation of triblock copolymer creating 1D nanostructures is still rare.[34] Therefore, the fabrication of 1D nanostructures via block copolymer self-assembly remains a challenge. In addition, the nonequilibrium conditions like shear

[a] Institute of Chemical Materials, Chinese Academy of Engineering and Physics, 621010 Mianyang, China. E-mail: zhouy@caep.cn.
[b] The 1st Affiliated Hospital of Dalian Medical University, 116000 Dalian, China. E-mail: xia_honggang@126.com.
[c] School of Mechanical and Electrical Engineering, Beijing Institute of Technology, Beijing, 100081, China.

† Electronic Supplementary Information (ESI) available: [All equilibrium micelle morphologies]. See DOI: 10.1039/x0xx00000x

flow are commonly encountered during processing. The understanding of shear-induced self-assembly of block copolymers has attracted a lot of attention.[35-37] Considering the ability of shear flow, i.e., the new assembled morphologies of block copolymers and the different orientation, we believe that the shear should be an effective approach to create 1D nanostructures of linear ABC triblock copolymers, which has not been preformed, to the best of our knowledge.

In this paper, we provide the first simulation of shear-induced morphologies of linear ABC triblock copolymers with different block sequences and block lengths by the DPD technique, and demonstrate that the shear is a good means of tailoring 1D cylindrical micellar structures based on our simulated whole morphological space.

2. Method and Model Details

DPD is a coarse-grained particle-based simulation technique, which allows the larger length and longer time scale. DPD particles obey Newton's equation of motion, and the forces between pair non-bonded DPD particles include a conservative force $\boldsymbol{F^C}$, a dissipative force $\boldsymbol{F^D}$, and a random force $\boldsymbol{F^R}$, respectively. A string of DPD particles bonded by a harmonic spring force $\boldsymbol{F^S}$ are always used to describe the polymer. Therefore, the total force is expressed by

$$f_i = \sum_{i \neq j} (F_{ij}^C + F_{ij}^D + F_{ij}^R + F_{(i,i+1)}^S) \quad (1)$$

The four forces are respectively given by

$$\begin{aligned} F_{ij}^C &= -a_{ij} w^C(r_{ij}) \mathbf{e}_{ij} \\ F_{ij}^D &= -\gamma w^D(r_{ij})(\mathbf{e}_{ij} \cdot \mathbf{v}_{ij}) \mathbf{e}_{ij} \\ F_{ij}^R &= \sigma w^R(r_{ij}) \xi_{ij} \Delta t^{-0.5} \mathbf{e}_{ij} \\ F_{(i,i+1)}^S &= -\sum_i k_S (l_{(i,i+1)} - l_0) \end{aligned} \quad (2)$$

where $\mathbf{r}_{ij}=\mathbf{r}_i-\mathbf{r}_j$, $r_{ij}=|\mathbf{r}_{ij}|$, $\mathbf{e}_{ij}=\mathbf{r}_{ij}/r_{ij}$ and $\mathbf{v}_{ij}=\mathbf{v}_i-\mathbf{v}_j$. ζ_{ij} is a Gaussian random number with zero mean and unit variance. α_{ij} is the repulsion parameter between bead i and j, which reflects the chemical characteristics of interacting beads. γ and σ are the friction constant and noise strength, respectively. For ensuring the system to satisfy the fluctuation-dissipation theorem and correspond to the Gibbs Canonical ensemble, only one of the two weight functions w^D and w^R can be chosen arbitrarily and this choice fixes the other one. There is also a relation between the amplitudes (σ and γ) and k_BT. It is $w^D=(w^R)^2$ and $\sigma^2=2\gamma k_BT$, k_B is the Boltzmann constant and T is the temperature.[38] A simple form for $w^C=(1-r_{ij})^2=w^D=(w^R)^2$ and $\sigma=3$ (*i.e.* $\gamma=4.5$) are chosen, and Newton equations for all beads are integrated by a modified version of the velocity-Verlet algorithm with $\lambda=0.65$.[39] In addition, $l_{(i,i+1)}$ is the bond length between connected two bead i and $i+1$. Here, the spring coefficient $k_S=4$ and the balance bond length $l_0=0$ are chosen. For easy numerical handling, the cutoff radius (r_c), the bead mass (m), and the temperature (k_BT) are chosen as the unit of the simulated system.

Figure 1 gives our coarse-grained models for *l*-ABC (*x*-*y*-*z*), *l*-BAC (*y*-*x*-*z*) and *l*-ACB (*x*-*z*-*y*) are consisted of the solvophilic block (A), the weakly solvophobic block (B) and the strongly solvophobic block (C), *x*, *y* and *z* are the number of bead A, B and C, respectively. The solvent is represented by an individual bead *S*. As for the interaction parameters (Table 1), we still follow those used by our previous works,[20-22] which are firstly defined to describe the self-assembly of the experimental miktoarm terpolymer.[6,8] However, Sheng *et al* think that the interactions between the poly(perfluoropropylene oxide) (F) block and other two blocks are very strong and provide a suite of gentle parameters.[10] Here, our main aim is to obtain the universal rule of governing shear-induced morphologies for *l*-ABC. Therefore, we still adopt these present parameters for better comparison with our previous works.

To avoid the finite size effect, our simulations are performed in a larger cubic box of size $(30r_c)^3$ containing 81000 DPD beads with random distribution at $\rho=3$. The Lees-Edwards periodic boundary condition is used to model shear flows and maintain a steady linear velocity profile with gradient $\tau=dv_x/dr_y$.[40,41] It also indicates that the shear direction is along the x axis. The different shear rate $\tau=0.01$, 0.05, 0.1, 0.15 and 0.2 are chosen to check the effect of shear rate on the morphologies. The concentrations (φ, the volume fraction) of *l*-ABC in solutions are 0.1, 0.2 and 0.3, respectively. The time step Δt is 0.03 and a total of $1\sim2\times10^6$ DPD time steps are carried out to guarantee the equilibration for each system.

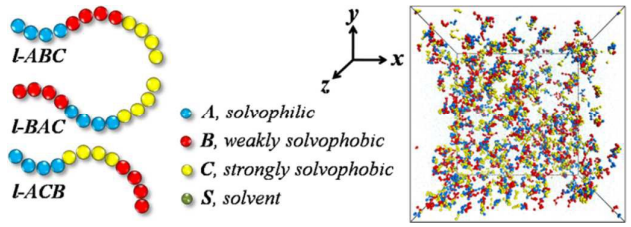

Fig. 1 The coarse-grained model of linear ABC triblock copolymers with different block sequences (left) and the simulation box with the initial constitution (right).

Table 1 Repulsion parameters (DPD unit) in this work

	A	B	C	S
A	25	45	90	27
B	45	25	75	50
C	90	75	25	120
S	27	50	120	25

3. Results and Discussions

The self-assemble morphology of ABC triblock copolymers in the solvent is controlled by a large parameter space, such as concentrations, block length and ratio, block sequences, interactions, and external factors (pH, temperature, pressure, shear, confined conditions, etc). Obviously, the expansive

parameter space can result in a boundless array of possible structures and further chemical functionalities. It is difficult to search one special structure among them. Therefore, we fixed all the interaction parameters and focused on the effect of shear rate (τ) and block length (*x*, *y and z*) on the morphology. For one of 3 sequences (*l*-ABC, *l*-BAC and *l*-ACB), there are 7 kinds of linear terpolymers with the different block length (2-2-2, 2-2-8, 2-8-2, 2-8-8, 8-2-2, 8-2-8 and 8-8-2), 5 kinds of shear rates (τ=0.01, 0.05, 0.1, 0.15 and 0.2) and 3 kinds of concentrations (φ=0.1, 0.2, 0.3). Considering all 3 sequences, a total of 315 equilibrium micellar morphologies (see ESI) are provided by our simulations. It is interesting that several shear-induced 1D cylindrical micelles are created.

Figure 2 gives five basic morphological schematics (sphere, oblate sphere, cylinder, oblate cylinder and lamella) summarizing from the full morphological phase diagrams (see ESI), which belong to three dimensionalities, respectively. It is a logical choice to ascribing the familiar spherical (dot), cylindrical (tube) and lamellar (sheet) micelles to zero-dimensional (0D), one-dimensional (1D) and two-dimensional (2D) structures, respectively. It is as same as the definition used by Bockstaller et al.[42] Specially, the oblate sphere and cylinder, comparing with the spherical (0D) and cylindrical (1D) micelles, show the obvious increase in the radical dimension and, therefore, are defined as 1D and 2D, respectively, which are more than the pristine structure. Next, we will introduce these morphologies with the different dimensionality according to the above classes in detail.

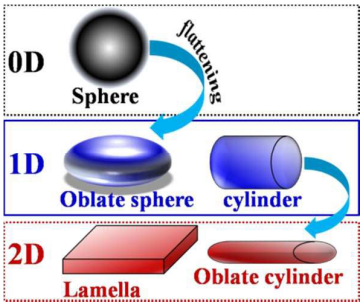

Fig. 2 Schematics for zero- (0D), one- (1D) and two-dimensional (2D) micellar structures by abstracting from all the phase diagrams.

For the 0D structure, about 8 types of spherical micelles are summarized from the whole phase diagram with 315 morphologies and the results are given in Figure 3. All these 0D spherical micelles have been found in our previous simulations[20-22] and other experiments.[14-18] For example, S_i^0, the typically concentric onion-like arrangement, does not have independent access to the exterior of the micelle. Judging from the appearance, S_{ii}^0, S_{iii}^0, S_{iv}^0 and S_v^0 are the familiar raspberry micelles. However, they have the complete different core, as shown in Figure 3. For example, S_v^0 is a big CSC micelle containing a small reverse CSC inside. However, S_{iii}^0 has only a core of B block.

As for the significant 1D structure, there are about 11 types of micellar morphologies created by the shear flow and drawn in Figure 4. Among them, all three micelles of oblate sphere (O_S^1), capsule (C_a^1) and worm (mC^1) in the first row are often provided by the common self-assembly of triblock copolymers in despite of shear flows. The following eight micelles with the notable cylinder characteristic are introduced in details: C_i^1 and C_{ii}^1 are the normal cylindrical core-shell-corona morphologies, the only difference is that the shell of the former is constitutive of B block and that of the latter is A block. C_{iii}^1 and C_{iv}^1 are the cylindrical CSC micelle with a cylindrical core. The core of C_{iii}^1 is C block and the shell of C_{iii}^1 is embedded by the dispersed C-rich domain, which is also found by concentration-induced self-assembly of linear ABC terpolymer in our previous study.[22] The difference between C_{iii}^1 and C_{iv}^1 is that the core of C_{iv}^1 is B block. C_v^1 and C_{vi}^1 are also regarded as the cylindrical CSC micelle. The difference with the typical one is that C_v^1 and C_{vi}^1 have two strips of shell, not like the continuous ones in the typical cylindrical CSC micelle. C_{vii}^1 is a single raspberry cylinder and C_{viii}^1 a gel of A block containing the different cylinder of B and C block, which is very similar to S_{vi}^0 and S_{vii}^0 in 0D structures. For the above 1D cylindrical micelles, if B and (or) C blocks can be selectively melted away, C_i^1 and C_{ii}^1 would change into the single-walled nanotube, and C_{iii}^1 and C_{iv}^1 would create the double-walled nanotube. The most interesting phenomenon is that C_{viii}^1 forms the paralleled co-micelle, which has been found from the self-assembly of PFS block copolymers.[32]

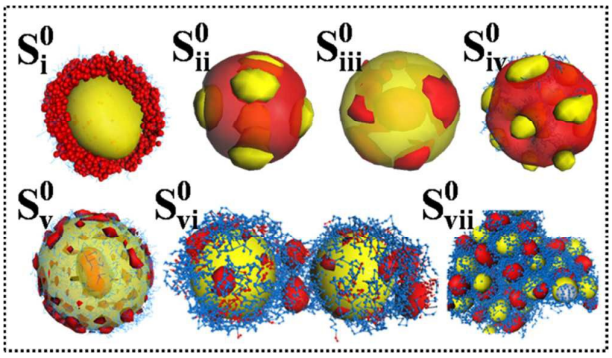

Fig. 3 Morphologies represented by the symbols for 0D micellar structures. Blue, red and yellow represents A-, B- and C-rich domains, respectively. For clarity, several morphologies use the isodensity surface and omit the A block. In symbols, **S** denotes the sphere, a superscript **0** represents 0D and the subscripts (**i-vii**) represent the different morphologies. **i**, spherical core-shell-corona (CSC) micelle; **ii**, raspberry micelle; **iii**, raspberry with a core of A block; **iv**, raspberry with a core of C block; **v**, a big CSC micelle containing a small CSC inside; **vi** and **vii**, spheres with different sizes in gel.

Among all 8 kinds of 2D structures in Figure 5, L_i^2 and L_{ii}^2 are the typical five layers morphology, which have the different order of ACBBCA (L_i^2) and ABCCBA (L_{ii}^2), respectively. L_{iii}^2 is a lamella like L_i^2, the difference is that the left three layers of L_{iii}^2 show a bend due to the variation of interfacial tension. mL_i^2 is a one-piece lamella consisting of alternant solvophobic blocks B and C (layers) linked by the solvophilic block A, and the thickness of single layer (B or C) is about a third of the lamella. As for mL_{ii}^2, it has not the average thickness and shows a spindle-like structure from the side view. Oc_i^2, as a normal oblate cylindrical micelle, can be regarded as a typical cylinder

flattened by external force. Oc_{ii}^{2} has a little variation, i.e., two cylindrical cores of B block. Obviously, Oc_{iii}^{2} is a curving oblate cylinder. Obviously, for the outer shapes of 2D structures, the interfacial tension plays a crucial role. Among them, L_{iii}^{2}, Oc_{ii}^{2} and Oc_{iii}^{2} are the production depending on the shear flow.

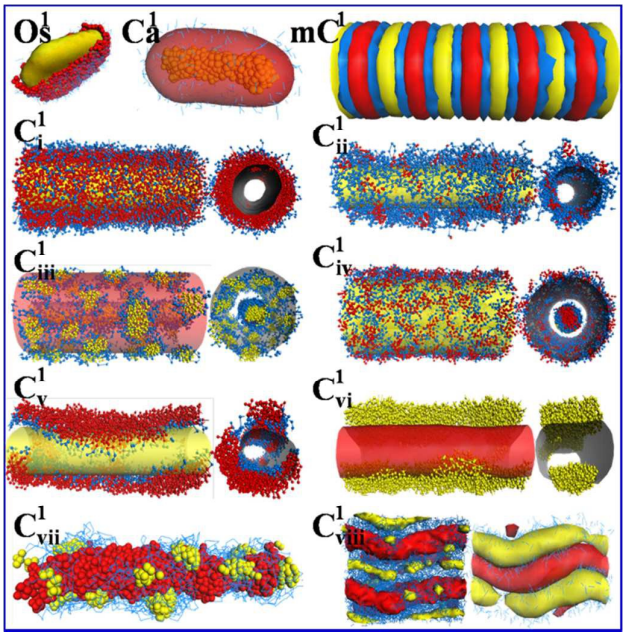

Fig. 4 Morphologies represented by the symbols for 1D micellar structures. Blue, red and yellow represents A-, B- and C-rich domains, respectively. For clarity, several morphologies use the isodensity surface and omit the A block. In symbols, **Os**, **Ca**, **mC** and **C** denote the oblate sphere, capsule-like, multicore and cylinder morphologies, respectively. A superscript **1** represents 1D and the subscripts (**i-viii**) represent the different cylinder structures. **i** and **ii**, cylindrical CSC with different shells; **iii**, cylindrical raspberry micelle with a cylindrical core of A and C block; **iv**, cylindrical micelle with a cylindrical core of A and B block; **v**, two strips of B block are linked to a cylindrical core of C block by A block; **vi**, two strips of C block are pasted on a cylindrical core of B block; **vii**, single raspberry cylindrical micelle; **viii**, different cylinders in the gel. For portions, the side view is given in right.

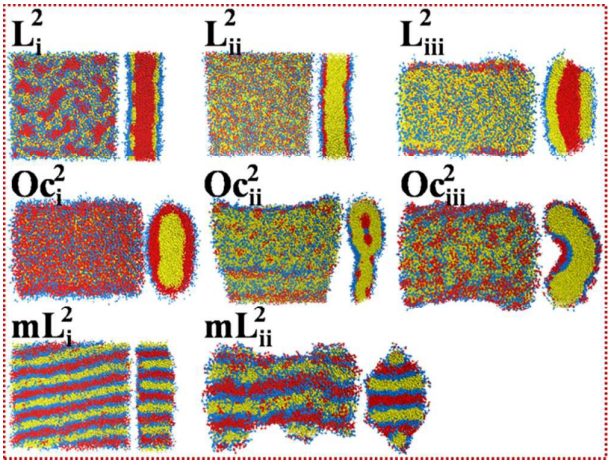

Fig. 5 Morphologies represented by the symbols for 2D structures. Blue, red and yellow represents A-, B- and C-rich domains, respectively. In symbols, **L**, **Oc** and **mL** denote the lamella, oblate cylinder and multi-layer morphologies, respectively. A superscript **2** represents 2D and the details on subscripts (**i-iii**) are given as follow: for Lamella, **i** and **ii**, lamella with a middle of block B and C, respectively; **iii**, lamella with a curving shell. For Oblate Cylinder, **i**, flat cylindrical CSC micelle with a core of block C; **ii**, flat cylindrical CSC with two parallel cores of block B; **iii**, curving flat cylindrical CSC with a core of block C. For multi-layer, **i**, alternate blocks A, B and C form a lamella; **ii**, alternate blocks A, B and C form a plump lamella. The side view is given in right.

Next, based on the above simple and direct class in Figure 2, we provide the whole morphological phase diagram for linear ABC triblock copolymers under the different concentrations and shear flows, and the results are shown in Figure 6 and 7, respectively. Meanwhile, we also select the given region in the phase diagrams of φ=0.1 (see the rectangles in Figure 6) and enlarge them for gaining the more detailed morphological information labelled by the symbols of Figure 3~5 (see the right of Figure 6). Although solution self-assembly of block copolymers represents one of the most promising approaches to prepare well-defined nanostructures with different shapes,[33] the formation of non-centrosymmetric 1D or 2D nanostructure remains a major challenge. At present, there is a small quantity of experiments[33,34,43] and simulations[22,44,45] on the aggregation of triblock copolymers that luckily access to approximate 1D structures. However, it is very rare for triblock copolymer to volume-produce 1D nanostructures. On the other hand, we all know that shear flow can change the orientation of the microphase to create globally aligned structures.[35,36] Therefore, we firstly utilize the shear flow to control the self-assembly of linear ABC terpolymers in solutions and introduce the fabrication of 1D structures. From the foregoing simulation morphologies, we have delightedly found several novel 1D cylindrical micelles. Then, by analyzing the phase diagrams of Figure 6 and 7, the elementary judgements in the mass are summarized as follows. Firstly, compared with our previous simulation without shear,[22] the area of phase diagrams held by the blue oblate spheres and cylinders (the so-called 1D structures) show a prominent increase, especially for the larger shear rate ($\tau \geqslant 0.1$). For example, in Figure 6c, all *l*-BAC triblock copolymers (including all 7 block compositions) form the 1D cylindrical morphologies after the shear rate is more than 0.1 ($\tau \geqslant 0.1$). It is also worth noting that, among these 1D structures, the numbers of cylindrical micelles are far more than those of oblate spheres. The widely blue domains dominating the phase diagrams richly testify that introducing the shear is a successful alternative as external stimuli to create a batch of cylindrical 1D structure in virtue of the advantage of solution self-assembly of linear ABC triblock copolymers. Secondly, as shown in Figure 6 and 7, it is clear that the dark sphere defined as 0D structure occupies the limited domain in phase diagrams, which mainly converge in the small shear rate ($\tau \leqslant 0.05$). The other interesting phenomenon is that the linear ABC terpolymers with the longer solvophilic A block have much ability to keep the spherical morphology when increasing the shear rate. In fact, those terpolymers with longer solvophilic A block prefer to form S_{vi}^{0} and S_{vii}^{0} structures that B and C block assembles the unattached spheres distributing in the gels of A block and the different ratio of B and C block would result in the different spherical size. Obviously, the longer solvophilic A block can build the powerful shield against the effect of solvent and

shear on the morphology, and the protected B and C block can easily go through the formation pathway of nucleation and growth.[22] However, the longer solvophilic A block can bring positive factors to play only for the smaller shear rate. Once the shear rate exceeds a given value, the system would self-assemble into the 1D structure like C^1_{viii}, whose B and C block turns into the different cylinders distributing in the gels of A block. For example, *l*-BAC (2-8-2) at φ=0.1 forms the 0D morphology of S^0_{vii} when the shear rate $\tau \leqslant 0.05$. Whereas we further increase the shear rate (τ=0.1), the 1D morphology of C^1_{viii} appears. The sphere-embedded gel configuration of ABC terpolymers[46] and its application in the drug release[2] have been given more and more attention. As for the cylinder-embedded gel configuration, the corresponding report is still rare, to the best of our knowledge. Thirdly, no matter what the block sequences, the so-called 2D structures including the oblate cylinder and the lamella also occupy the relative marked domain in phase diagrams shown in Figure 7, mainly for the larger concentration of φ=0.2 and 0.3. For example, the phase diagrams of *l*-ACB drawn in Figure 6a and 7a, respectively, show a considerable amount of differences. In details, all the *l*-ACB (*x*-*z*-*y* is equal to 2-2-2, 2-2-8 and 2-8-2) terpolymers at φ=0.2 (Figure 7a) assemble to the oblate cylindrical micelles under all the shear rates, however, at φ=0.1 (Figure 6a) they form the same oblate cylindrical micelle only under four conditions, i.e., *x*-*z*-*y* is 2-8-2 and τ=0.15, *x*-*z*-*y* is 2-2-2 and τ=0.1, 0.15 and 0.2, respectively. In addition, compared with the oblate cylinder, the lamellar morphologies are more frequently found at the concentration of φ=0.3.

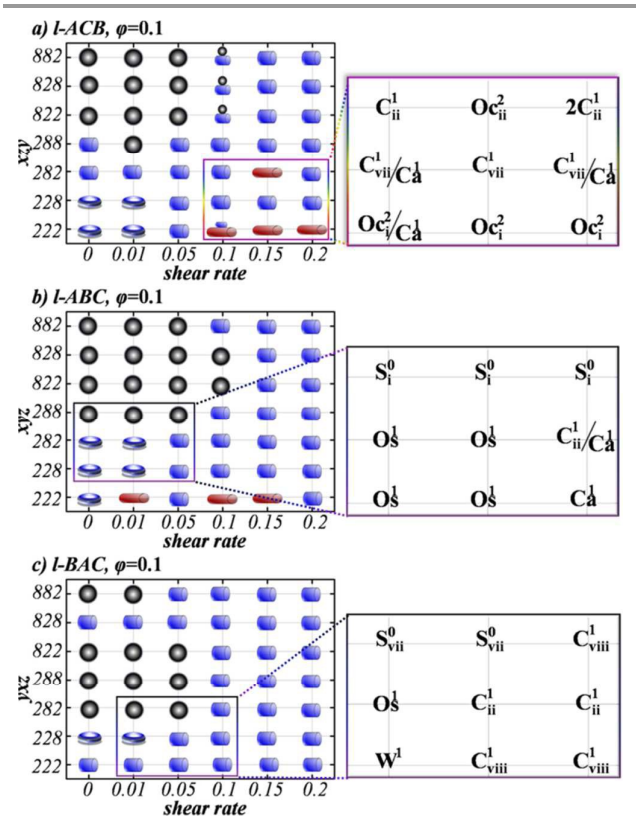

Fig. 6 Morphological phase diagrams of linear ABC terpolymers under the different shear rate at the concentration φ=0.1. The three numbers listed in y-axis represent the length of block A, B and C, respectively. The values of x-axis are the different shear rate. The right detailed phase diagrams are the results after the part in left quadrangle are enlarged.

Taking *l*-ACB (2-2-2, 2-2-8 and 2-8-2) under τ=0.01 as examples, for *l*-ACB (2-2-2 and 2-2-8) terpolymers they provide the oblate spherical morphology at φ=0.1 (Figure 6a), the oblate cylindrical ones at φ=0.2 (Figure 7a) and the lamellar ones at φ=0.3 (Figure 7d), respectively. The *l*-ACB (2-8-2) experiences the morphological variation from the cylinder to the oblate cylinder and the lamella with the increase of the concentration from 0.1 to 0.3. In fact, the oblate cylindrical micelle is not the specific product of shear-induced self-assembly of ABC triblock copolymers, and in the concentration-induced morphologies it is also expressed frequently.

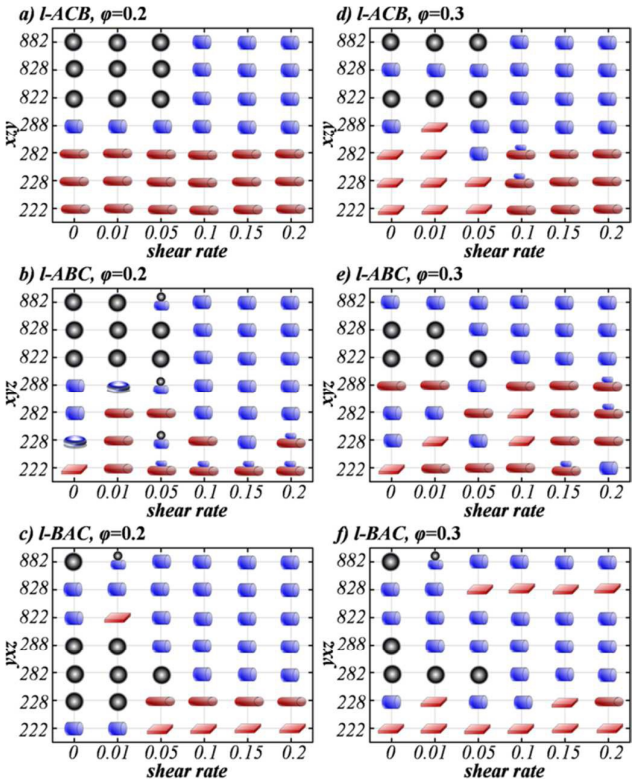

Fig. 7 Morphological phase diagrams of linear ABC terpolymers under the different shear rate at the concentration φ=0.2 and 0.3. The three numbers listed in y-axis represent the length of block A, B and C, respectively. The values of x-axis are the different shear rate.

Finally, the long-coexistence of different morphological micelles, such as sphere/cylinder and cylinder/oblate cylinder, often appears in phase diagrams of Figure 6 and 7. It has to emphasise that each schematic shape (sphere, oblate sphere, cylinder, oblate cylinder and lamella) in Figure 2 corresponds to a series of different morphologies. For example, the dark sphere represents an aggregate of seven 0D morphologies in Figure 3, and the blue cylinder is a deputation containing ten 1D cylinder-like morphologies (except for the oblate sphere O^1_S)

in Figure 4. Therefore, we can zoom in the phase diagrams like the right portion of Figure 6 to search more coexistent micelles. It is interesting that the more mixtures of two similar morphologies, such as C_{vii}^{1}/C_{a}^{1}, Oc_{i}^{2}/C_{a}^{1} and C_{ii}^{1}/C_{a}^{1}, can be searched. The phase diagrams in Figure 7 can also find much coexistent morphologies like the above mentioned, if we display them based on the detailed morphological symbols (in Figure 3~5), not the schematic shapes (in Figure 2). Of course, our provided 315 equilibrium micellar morphologies in the electronic supporting information (ESI) can approximately support the above results.

Based on the above analyzed results, we can summarize several factors of influencing the creation of multidimensional micellar morphologies through the self-assembly of linear ABC terpolymers in solutions. The important one is the shear rate (τ). The reorientation and rearrange of the morphologies, which can easily result in the mass formation of 1D structure, significantly depend on the larger shear rate. However, the small shear rate (τ=0.01) hardly alter any morphologies, that is, very similar to those from solution self-assembly without shear. The next one is the concentration (φ). The larger concentration is a top priority to build the 2D structures (oblate cylinder and lamella). The lamellar morphologies are almost from the concentration of φ=0.2 and 0.3. At the small φ=0.1, there is a lack of the lamella for all linear ABC triblock copolymers and shear rates, and the limited numbers of the oblate cylinder only for *l*-ACB (2-2-2) and *l*-ABC (2-2-2). The last one is the length of the solvophilic A block. The longer solvophilic A block has the obvious shield ability and protect the self-assembly from the effect of solvents and shear rates (only in the given range), which is propitious to the formation of 0D spherical micelles like S_{vi}^{0} and S_{vii}^{0}.

Conclusions

In summary, combined with our previous works,[20-22] we further utilize DPD simulation method to give insight into the shear-induced self-assemble morphologies of linear ABC triblock copolymers in solutions, where A is a solvophilic block, B and C are weakly solvophobic and strong solvophobic blocks, respectively. The shear flow (introduced by the Lees-Edwards periodic boundary condition) has a remarkable influence on the morphologies, especially for the creation of 1D cylindrical micelles. The detail phase diagrams show that, the larger shear rate is a real key factor to fabricate the 1D structure and the smaller one hardly produces any influence. However, the shear rate is not the one and only factor of controlling the morphology, the concentration and the block length would play a significant role for the special structure. For example, the larger concentration is a preferential choice to obtain the 2D structure, especially the lamella. The longer solvophilic block prefers to help the formation of "spheres in gel" (0D). In addition, several 1D cylindrical micelles (such as $C_{i\sim viii}^{1}$) can be further processed (melting one or two blocks away) and should become the single-, double-walled nanotubes, and the cylindrical co-micelles, respectively. In fact, this work provides a simple and effective approach, which is that introducing the shear flow promotes the reorientation and rearrange of self-assemble morphologies, to selectively build 0D (dot), 1D (tube) or 2D (sheet) nanostructures. These results are helpful to understand the formation of complex micelles by the shear-induced self-assembly of linear ABC triblock copolymers, and can assist experiments to create the new 1D cylindrical morphologies.

Acknowledgements

All the authors appreciate very much the financial support from Foundation of CAEP (No.2014B0302040, 2014-1-075) and National Nature Sciences Foundation of China (No.11402241).

Notes and references

§ These authors contributed equally to this work.

1 I. W. Hamley, *Block Copolymers in Solution: Fundamentals and Applications*; Wiley: Hoboken, NJ, 2005.
2 M. K. Gupta, J. R. Martin, T. A. Werfel, T. W. Shen, J. M. Page and C. L. Duvall, *J. Am. Chem. Soc.*, 2014, **136**, 14896.
3 R. Ruiz, H. Kang, F. A. Detcheverry, E. Dobisz, D. S. Kercher, T. R. Albrecht, J. J. de Pablo and P. F. Nealey, *Science,* 2008, **321**, 936.
4 A. O. Moughton, M. A. Hillmyer and T. P. Lodge, *Macromolecules*, 2012, **45**, 2.
5 N. Hadjichristidis, H. Iatrou, M. Pitsikalis, S. Pispas and A. Avgeropoulos, *Prog. Polym. Sci.*, 2005, **30**, 725.
6 Z. Li, E. Kesselman, Y. Talmon, M. A. Hillmyer, and T. P. Lodge, *Science*, 2004, **306**, 98.
7 A. Laschewsky, *Curr. Opin. Colloid Interface Sci.*, 2003, **8**, 274.
8 J. Xia and C. Zhong, *Macromol. Rapid Commun.,* 2006, **27**, 1110.
9 Y. Zhao, Y. T. Liu, Z. Y. Lu and C. C. Sun, *Polymer*, 2008, **49**, 4899.
10 S. H. Chou, H. K. Tsao and Y. J. Sheng, *J. Chem. Phys.*, 2006, **125**, 194903.
11 E. B. Zhulina and O. V. Borisov, *Macromolecules*, 2008, **41**, 5934.
12 W. Kong, B. Li, Q. Jin, D. Ding and A. C. Shi, *J. Am. Chem. Soc.*, 2009, **131**, 8503.
13 S. Li, Y. Jiang and J. Z. Y. Chen, *Soft Matter*, 2013, **9**, 4843.
14 M. Kubowicz, J. F. Baussard, J. F. Lutz, A. F. Thunemann, H. von Berlepsch and A. Laschewsky, *Angew. Chem., Int. Ed.*, 2005, **44**, 5262.
15 H. von Berlepsch, C. Bottcher, K. Skrabania and A. Laschewsky, *Chem. Commun.*, 2009, **17**, 2290.
16 K. Skrabania, A. Laschewsky, H. von Berlepsch and C. Bottcher, *Langmuir*, 2009, **25**, 7594.
17 K. Skrabania, H. von Berlepsch, C. Bottcher and A. Laschewsky, *Macromolecules*, 2010, **43**, 271.
18 J. N. Marsat, M. Heydenreich, E. Kleinpeter, H. von Berlepsch, C. Bottcher and A. Laschewsky, *Macromolecules*, 2011, **44**, 2092.
19 E. Betthausen, C. Hanske, M. Müller, A. Fery, F. H. Schacher, A. H. E. Müller and D. J. Pochan, *Macromolecules,* 2014, **47**, 1672.
20 Y. Zhou, H. G. Xia, X. P. Long, X. G. Xue and W. Qian, *Macromol. Theory Simul.,* 2015, **24**, 85.
21 Y. Zhou, X. P. Long, X. G. Xue, W. Qian and C. Y. Zhang, *RSC Adv.*, 2015, **5**, 7661.

22 C. Zhou, H. G. Xia, Y. Zhou, X. G. Xue and S. K. Luo, *RSC Adv.*, 2015, **5**, 58024.
23 L. Wang and J. P. Lin, *Soft Matter*, 2011, **7**, 3383.
24 J. Xin, D. Liu and C. L. Zhong, *J. Phys. Chem. B,* 2009, **113**, 9364.
25 U. Nagpal, F. A. Detcheverry, P. F. Nealey and J. J. de Pablo. *Macromolecules,* 2011, **44**, 5490.
26 Y. T. Zhu, X. P. Yang, W. X. Kong, Y. P. Sheng and N. Yan, *Soft Matter*, 2012, **8**, 11156.
27 L. Q. Wang and J. P. Lin, *Soft Matter*, 2011, **7**, 3383.
28 Y. Geng, P. Dalhaimer, S. Cai, R. Tsai, M. Tewari, T. Minko and D. E. Discher, *Nat. Nanotechnol.*, 2007, **2**, 249.
29 A. W. Fahmi, H. G. Braun and M. Stamm, *Adv. Mater.*, 2003, **15**, 1201.
30 M. Muellner, J. Yuan, S. Weiss, A. Walther, M. Foertsch, M. Drechsler and A. H. E. Mueller, *J. Am. Chem. Soc.*, 2010, **132**, 16587.
31 X. S. Wang, H. Wang, N. Coombs, M. A. Winnik and I. Manners, *J. Am. Chem. Soc.,* 2005, **127**, 8924.
32 X. Wang, G. Guerin, H. Wang, Y. Wang, I. Manners and M. A. Winnik, *Science*, 2007, **317**, 644.
33 P. A. Rupar, L. Chabanne, M. A. Winnik and I. Manners, *Science*, 2012, **337**, 559.
34 L. L. Wang, H. Y. Huang and T. B. He, *Macromol. Rapid Commun.*, 2014, **35**, 1387.
35 D. H. Liu and C. L. Zhong, *Macromol. Rapid Commun.,* 2005, **26**, 1960.
36 L. Y. You, L. J. Chen, H. J. Qian, and Z. Y. Lu, *Macromolecules*, 2007, **40**, 5222.
37 B. L. Peters, A. R. Hernandez, D. Q. Pike, M. Muller and J. J. de Pablo, *Macromolecules*, 2012, **45**, 8109.
38 P. Español and P. B. Warren, *Europhys. Lett.*, 1995, **30**, 191.
39 R. D. Groot and P. B. Warren, *J. Chem. Phys.*, 1997, **107**, 4423.
40 M. P. Allen and D. J. Tildesley, *Computer Simulation of Liquids* (Clarendon Press, Oxford, 1987).
41 A. W. Lees and S. F. Edwards, *J. Phys. C.*, 1972, **5**, 1921.
42 M. R. Bockstaller, R. A. Mickiewicz and E. L. Thomas, *Adv. Mater.,* 2005, **17**, 1331.
43 C. H. Luo, Y. Liu and Z. B. Li. *Soft Matter,* 2012, **8**, 2618.
44 Y. T. Zhu, H. Z. Yu, Y. M. Wang, J. Cui, W. X. Kong and W. Jiang,*Soft Matter,* 2012, **8**, 4695.
45 Y. T. Zhu, X. P. Yang, W. X. Kong, Y. P. Sheng and N. Yan, *Soft Matter,* 2012, **8**, 11156.
46 C. Zhou, M. A. Hillmyer and T. P. Lodge, *J. Am. Chem. Soc.,* 2012, **134**, 10365.

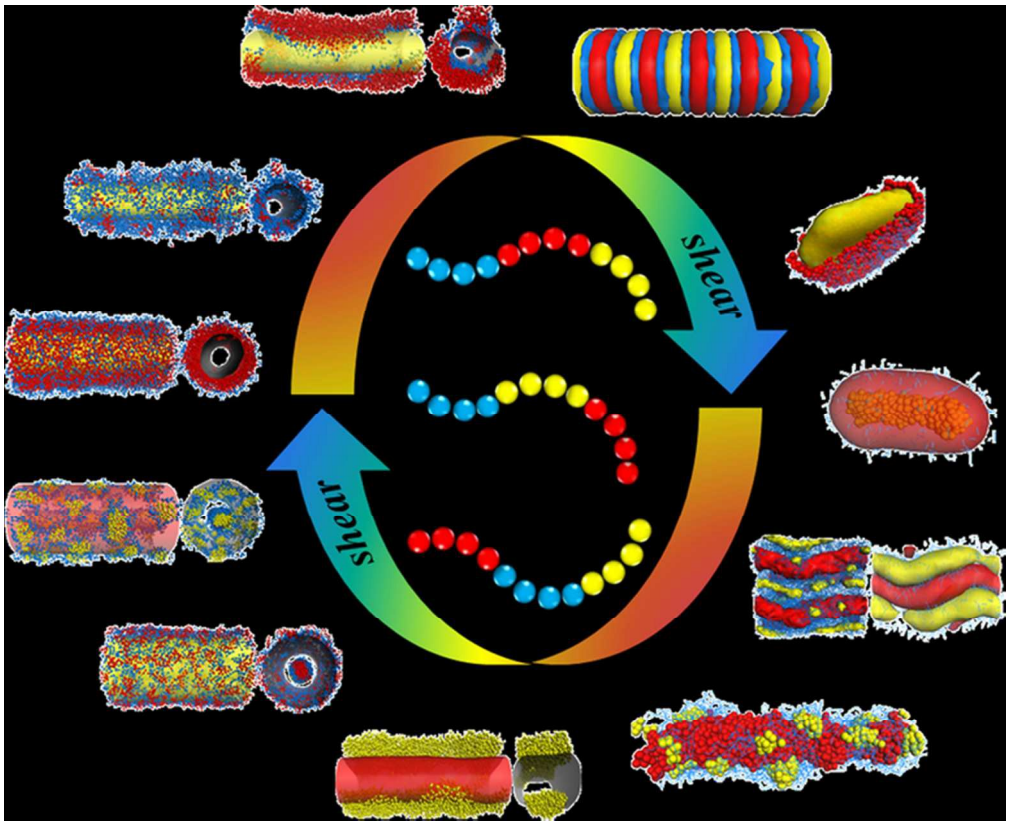

65x53mm (300 x 300 DPI)